Assessing the Calibration of High-Dimensional Ensemble Forecasts Using Rank Histograms

Thordis L. Thorarinsdottir*, Michael Scheuerer† and Christopher Heinz‡

Abstract

Any decision making process that relies on a probabilistic forecast of future events necessarily requires a calibrated forecast. This paper proposes new methods for empirically assessing forecast calibration in a multivariate setting where the probabilistic forecast is given by an ensemble of equally probable forecast scenarios. Multivariate properties are mapped to a single dimension through a pre-rank function and the calibration is subsequently assessed visually through a histogram of the ranks of the observation's pre-ranks. Average ranking assigns a pre-rank based on the average univariate rank while band depth ranking employs the concept of functional band depth where the centrality of the observation within the forecast ensemble is assessed. Several simulation examples and a case study of temperature forecast trajectories at Berlin Tegel Airport in Germany demonstrate that both multivariate ranking methods can successfully detect various sources of miscalibration and scale efficiently to high dimensional settings. Supplemental material in form of computer code is available online.

Keywords: average rank; band depth; forecast trajectory; forecast verification; modified band depth; multivariate forecast

*Norwegian Computing Center, Oslo, Norway. *Corresponding author: thordis@nr.no*
†National Ocean and Atmospheric Administration, Boulder, Colorado, U.S.A.
‡Faculty of Mathematics and Economics, Ulm University, Germany.

1 Introduction

Calibration, the statistical compatibility between a probabilistic forecast and the realized observation, is a fundamental property of any skillful forecast. Formally, we say that the forecast is calibrated if, over the long run, events assigned a given probability are realized with the same empirical frequency. Calibration is thus a critical requirement for optimal decision making and any decision aiding technique that relies on the forecast (Lichtenstein et al., 1977; Gneiting et al., 2007).

In the case of a univariate probabilistic forecast given by a continuous predictive distribution, Dawid (1984) proposes the use of the probability integral transform (PIT) for calibration assessment. That is, if F is the cumulative distribution function (CDF) of a calibrated probabilistic forecast for the observation y, it holds that $F(y) \sim \mathcal{U}([0, 1])$. A randomized version of the PIT that applies to partly, or fully, discrete distributions is discussed in Czado et al. (2009). For an ensemble of deterministic forecasts that approximate the predictive distribution, an equivalent tool is the rank of the observation y in the forecast ensemble $x_1, \ldots, x_{m-1}$ (Anderson, 1996; Hamill and Colucci, 1997). The calibration of a large number of forecast cases may then be assessed empirically by plotting the histogram of the resulting PIT values or verification ranks (Gneiting et al., 2007). If the forecasts lack calibration, the shape of the PIT or the verification rank histogram may reveal the nature of the misspecification and thus provide a useful guidance to the improvement of the forecasting method. For instance, a $\cup$-shaped histogram is an indication of underdispersion while a $\cap$-shape suggests overdispersion.

To assess the calibration of multivariate ensemble forecasts, Gneiting et al. (2008) propose a general two-step framework. In the first step, the observation and the ensemble members are assigned univariate pre-ranks. The rank of the observation is then given by the rank of its pre-rank. A multivariate calibration technique based on minimum spanning trees proposed by Smith and Hansen (2004) and Wilks (2004) seamlessly falls within this framework. Alternatively, Gneiting et al. (2008) propose a multivariate rank structure equal to that of the empirical copula. A recent extension that applies to full distributions is given in Ziegel and Gneiting (2013). While

the multivariate rank histogram has been shown to work well for low-dimensional forecasts, see e.g. Schuhen et al. (2012) and Möller et al. (2013), the multivariate ordering in the first step seems to lack power in higher dimensions (Pinson and Girard, 2012). Alternative methods for high-dimensional calibration assessment have thus been called for (Pinson, 2013; Schefzik et al., 2013).

We propose two pre-ranking methods that complement the techniques of Gneiting et al. (2008), Smith and Hansen (2004) and Wilks (2004). The new methods are based on the concept of band depth for functional data introduced by López-Pintado and Romo (2009) which relates to the graphical representation of the functional data curves. That is, continuous or discrete curves are given a center-outward ordering according to the centrality of a curve within the collection of sample curves. Sun and Genton (2011, 2012) apply this concept to develop a box plot for the visualization and outlier-detection of functional data. Viewing a discrete curve of length d as a point in d-dimensional space, we define a pre-ranking method based on the band depth concept of López-Pintado and Romo (2009). In the discrete case, the band depth essentially corresponds to the average centrality of the d points. As a second alternative, we thus also consider a pre-rank given by the average of the univariate ranks.

The remainder of the paper is organized as follows. In Section 2, we review the concept of band depth for discrete data and define the two multivariate ranking methods. Section 3 and 4 provide the results of simulation studies where we investigate the influence of dimensionality and correlation, respectively, on the band depth ranks, the average ranks and the two previously proposed techniques. A further comparison of the four techniques is provided in Section 4, where we assess the calibration of temporal trajectories of temperature forecasts over Germany. The paper then ends with a discussion in Section 5.

2 Ranking multivariate data

Let $S = \{\mathbf{x}_1, \dots \mathbf{x}_m\}$ denote a set of points in $\mathbb{R}^d$ or a d-dimensional subset thereof, with $\mathbf{x}_i = (x_{i1}, \dots, x_{id})$. Here, we can think of S as comprising an ensemble forecast with $m-1$ ensemble members and the corresponding observation $\mathbf{y} = \mathbf{x}_m$. Following the general set-up of Gneiting et al. (2008), the rank of the observation in S is calculated in two steps,

(i) apply a pre-rank function $\rho_S : \mathbb{R}^d \to \mathbb{R}_+$ to calculate the pre-rank, $\rho_S(\mathbf{x})$, of every $\mathbf{x} \in S$;

(ii) set the rank of the observation $\mathbf{x}_m$ equal to the rank of $\rho_S(\mathbf{x}_m)$ in $\{\rho_S(\mathbf{x}_1), \dots, \rho_S(\mathbf{x}_m)\}$ with ties resolved at random.

Under minimum spanning tree ranking, the pre-rank function $\rho_S^{\text{mst}}(\mathbf{x})$ is given by the length of the minimum spanning tree of the set $S \setminus \mathbf{x}$ (Smith and Hansen, 2004; Wilks, 2004). Here, a spanning tree of the set $S \setminus \mathbf{x}$ is a collection of $m-2$ edges such that all points in $S \setminus \mathbf{x}$ are used. The spanning tree with the smallest length is then the minimum spanning tree (Kruskal, 1956); it may e.g. be calculated using the `R` package `vegan` (R Core Team, 2013). The multivariate ranking of Gneiting et al. (2008), on the other hand, is defined using the pre-rank function

$$\rho_S^{\text{m}}(\mathbf{x}) = \sum_{i=1}^{m} \mathbb{1}\{\mathbf{x}_i \preceq \mathbf{x}\}, \tag{1}$$

where $\mathbb{1}$ denotes the indicator function and $\mathbf{x}_i \preceq \mathbf{x}$ if and only if $x_{ik} \leq x_k$ for all $k = 1, \dots, d$. Gneiting et al. (2008) further consider an optional initial step in the ranking procedure in which the data is normalized in each component before the ranking. As the pre-rank functions proposed below are invariant to such pre-processing, we omit this step here.

2.1 Band depth rank

López-Pintado and Romo (2009) introduce a center-outward ordering of curves which they call band depth. In the discrete case, it is defined as the proportion of coordinates of $\mathbf{x} \in S$ inside

bands defined by subsets of n points from S,

$$\mathrm{bd}_S^n(\mathbf{x}) = \binom{m}{n}^{-1} \frac{1}{d} \sum_{k=1}^{d} \sum_{1 \le i_1 < \ldots < i_n \le m} \mathbb{1}\big\{ \min\{x_{i_1 k}, \ldots, x_{i_n k}\} \le x_k \\ \times \mathbb{1}\big\{ x_k \le \max\{x_{i_1 k}, \ldots, x_{i_n k}\} \quad . \tag{2}$$

Note that López-Pintado and Romo (2009) refer to this version of the definition as modified band depth, in reference to the corresponding definition for continuous curves. It holds that $0 \le \mathrm{bd}_S^n(\mathbf{x}) \le 1$ for all $\mathbf{x} \in S$ and it gets closer to 1 the deeper, or more central, the point $\mathbf{x}$ is in the set S. Previous studies note that the resulting ordering of the elements in S is robust to changes in the value of n and we thus only consider the case $n = 2$ which is equal to the simplical depth of Liu (1990) and computationally very efficient (López-Pintado and Romo, 2009; Sun et al., 2013).

From (2), we obtain the band depth pre-rank function

$$\begin{aligned} \rho_S^{\mathrm{bd}}(\mathbf{x}) &= \frac{1}{d} \sum_{k=1}^{d} \sum_{1 \le i_1 < i_2 \le m} \mathbb{1}\big\{ \min\{x_{i_1 k}, x_{i_2 k}\} \le x_k \le \max\{x_{i_1 k}, x_{i_2 k}\} \\ &= \frac{1}{d} \sum_{k=1}^{d} \Big[\mathrm{rank}_S(x_k) \big[m - \mathrm{rank}_S(x_k) \big] + \big[\mathrm{rank}_S(x_k) - 1 \big] \sum_{i=1}^{m} \mathbb{1}\{x_{ik} = x_k\} \Big], \end{aligned} \tag{3}$$

where $\mathrm{rank}_S(x_k) = \sum_{i=1}^{m} \mathbb{1}\{x_{ik} \le x_k\}$ denotes the rank of the kth coordinate of $\mathbf{x}$ in S. If $x_{ik} \ne x_{jk}$ with probability 1 for all $i, j \in \{1, \ldots m\}$ with $i \ne j$ and $k = 1, \ldots, d$, the band depth pre-rank function in (3) further simplifies to

$$\rho_S^{\mathrm{bd}}(\mathbf{x}) = \frac{1}{d} \sum_{k=1}^{d} \big[m - \mathrm{rank}_S(x_k) \big] \big[\mathrm{rank}_S(x_k) - 1 \big] + (m - 1), \tag{4}$$

see also Sun et al. (2013).

It is straightforward to see that the band depth rank of an observation $\mathbf{y} = \mathbf{x}_m$ is uniformly distributed if $\mathbf{x}_1, \ldots, \mathbf{x}_m$ are independent and identically distributed, which implies a calibrated ensemble forecast. However, the interpretation of the resulting rank histogram is somewhat differ-

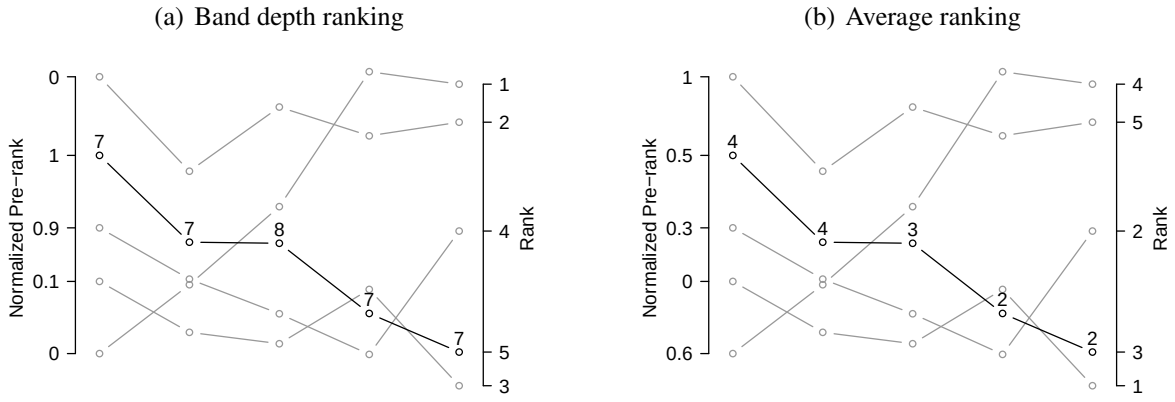

Figure 1: Illustration of (a) band depth, and (b) average pre-ranking for a multivariate temporal trajectory with $d = 5$ time points. The normalized pre-ranks of each curve are given on the left and the resulting ranks on the right. The four ensemble forecast curves are indicated in gray and the observation curve in black. The numbers next to each point of the observation curve indicate the univariate pre-ranks.

ent than that of the classical univariate verification rank histogram. As the example in Figure 1(a) shows, the band depth pre-rank assesses the centrality of the elements in S, with the most central element(s) attaining the highest rank(s) and the most outlying element(s) attaining the lowest rank(s). A skew histogram with too many high ranks is thus an indication of an overdispersive ensemble while too many low ranks can result from either an underdispersive or biased ensemble. As demonstrated in the simulation study in Section 4, a lack of correlation in the ensemble will result in a $\cup$-shaped histogram while an ensemble with too high correlations produces a $\cap$-shaped histogram.

2.2 Average rank

The average rank is simply given by the average over the univariate ranks,

$$\rho_S^{\mathrm{a}}(\mathbf{x}) = \frac{1}{d} \sum_{k=1}^{d} \mathrm{rank}_S(x_k). \tag{5}$$

An illustration of the average pre-ranking is given in Figure 1. It follows directly from (5) that the resulting rank of the observation $\mathbf{x}_m$ in S is uniform on $\{1, \ldots, m\}$ if the elements of S are independent and identically distributed. The average rank furthermore reduces to the classical

univariate rank when $d = 1$.

The interpretation of the resulting histogram is similar to that of the univariate verification rank histogram. That is, if the forecasts are underdispersive the average rank histogram for the observation is $\cup$-shaped, an overdispersive ensemble results in a $\cap$-shaped histogram while a constant bias results in a triangular shaped histogram. As discussed in Section 4 under- and overestimation of the correlation structure can furthermore result in over- and underdispersive histograms, respectively.

3 Histogram shape and the effect of dimensionality

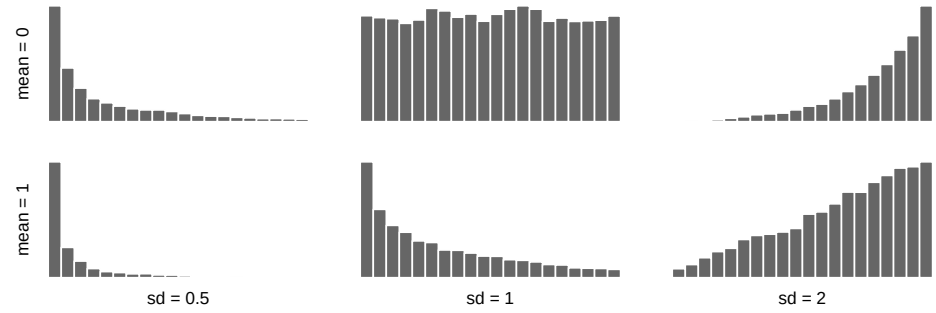

Figure 2: Band depth rank histograms for observations in $d = 3$ dimensions that follow independent standard Gaussian distributions while the 19 ensemble members follow independent Gaussian distributions with parameters as indicated. The results are based on 10000 repetitions.

To demonstrate the shape of the histograms subject to over- and underdispersion as well as bias, we consider a simple simulation experiment where the observations follow an independent standard Gaussian distribution in each dimension. Figure 2 shows band depth rank histograms under this model in a low dimensional setting with $d = 3$ and $m = 20$. The ensemble forecasts are also assumed to follow independent Gaussian distributions with mean $\mu \in \{0, 1\}$ and standard deviation $\sigma \in \{0.5, 1, 2\}$. When the forecasts are underdispersive or have a constant bias, the observation curve is often among the most outlying curves resulting in too many low ranks. Similarly, if the forecasts are overdispersive, the observation curves are too central on average, resulting in too many high ranks. Figure 3 shows the average rank histograms for the same setting. Here, the interpretation of the average ranks is equivalent to that of the standard univariate rank

histogram. The histogram shape clearly indicates overdispersion in the forecast through a ∩-shape, underdispersion through a ∪-shape and bias via a skew, triangular shaped histogram.

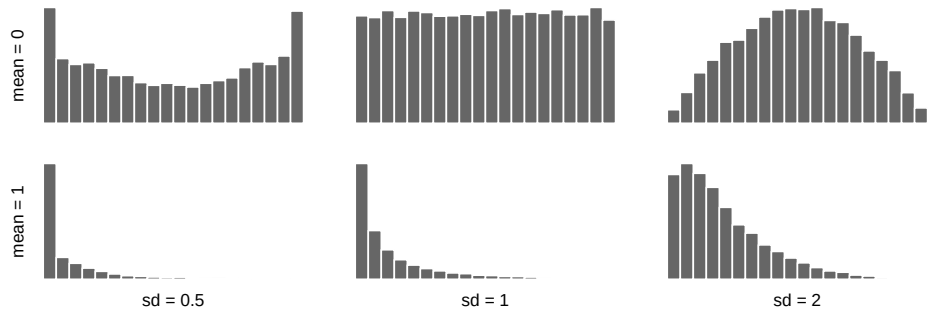

Figure 3: Average rank histograms for observations in $d = 3$ dimensions that follow independent standard Gaussian distributions while the 19 ensemble members follow independent Gaussian distributions with parameters as indicated. The results are based on 10000 repetitions.

Figure 4 and 5 demonstrate the effect of increasing dimensionality on the four multivariate ranking methods discussed in Section 2 subject to under- and overdispersion, respectively. While we still assume the ensemble consists of 19 members, the dimensionality of the data is here increased to 5 and 15 dimensions. This setting may seen somewhat extreme in that we attempt to represent the multivariate correlation structure in 15 dimensions with only 19 trajectories. However, this is common e.g. in atmospheric sciences, where due to computational limitations ensembles of similar magnitude are used to represent very high dimensional multivariate distributions.

The average rank histograms for both examples appear unchanged compared to the low dimensional example in Figure 3 while for the band depth rank, the evidence of miscalibration seem to get stronger with higher dimensions. The minimum spanning tree ranking provides a center-outward ordering of the curves similar to statistical depth functions (Gneiting et al., 2008; Zuo and Serfling, 2000) and for the examples here, the shape of the minimum spanning tree rank histograms is nearly identical to that of the band depth rank histograms. As reported in Pinson and Girard (2012), we observe identifiability issues with the multivariate ranking of Gneiting et al. (2008) in higher dimensions. In 5 dimensions, only the upper half of the ranks indicates miscalibration and the multivariate rank histograms appear close to uniform when $d = 15$ even though the forecasts are severely miscalibrated. The reason for this can be seen by considering the example in Fig-

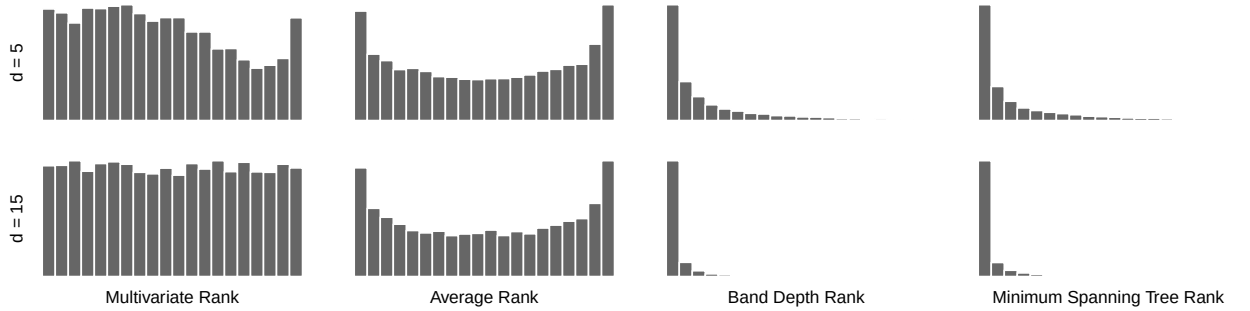

Figure 4: Multivariate ranking of observations in dimension $d = 5$ (top row) and $d = 15$ (bottom row) that follow independent standard Gaussian distributions when the 19 ensemble member forecasts are underdispersed following independent zero-mean Gaussian distributions with standard deviation of 0.5.

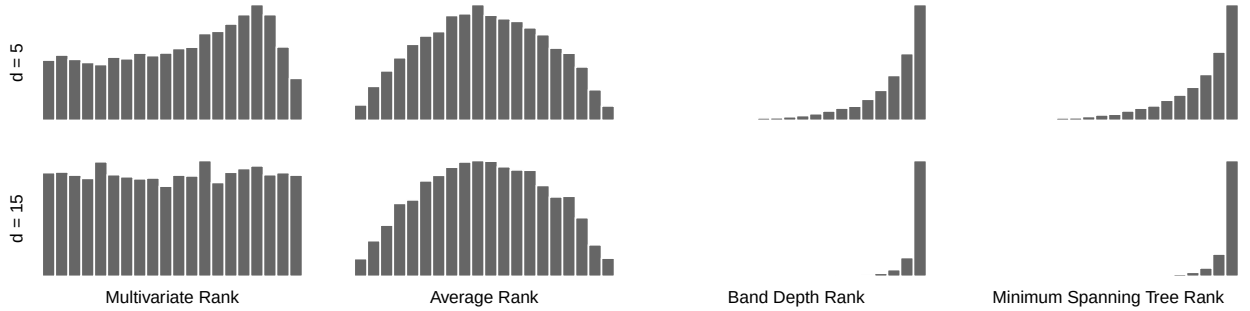

Figure 5: Multivariate ranking of observations in dimension $d = 5$ (top row) and $d = 15$ (bottom row) that follow independent standard Gaussian distributions when the 19 ensemble member forecasts are overdispersed following independent zero-mean Gaussian distributions with standard deviation of 2.

ure 1, where, due to crossing of the curves, four out of the five curves would obtain a multivariate pre-rank of 1.

Additional simulation studies show that miscalibration is generally easier to detect in larger ensembles than in small ensembles (results not shown). While these results holds across the different pre-ranking techniques, it appears that the curse of dimensionality observed for the multivariate ranking in Figures 4 and 5 cannot be avoided by increasing the size of the forecast ensemble. Computer code to recreate Figures 2-5 using `R` (R Core Team, 2013) is available in the online supplementary material.

4 Assessing deviations in the correlation structure

An appropriate modeling of the correlation between the different components is an important aspect of multivariate predictions. It is not entirely obvious from their definition why the band depth and the average rankings are sensitive to misspecification of the correlation structure. This can be demonstrated by comparing the variances of the pre-ranks under different dependence strengths. First, consider the extreme case where the observations are fully dependent (i.e. identical) and the forecasts are independent across the different components. Assuming, as before, that the different curves are pairwise independent, the rank of the ith random curve $\mathbf{X}_i$ is uniformly distributed on $\{1, \dots, m\}$ for each component $k = 1, \dots, d$. Under the pre-rank functions in (4) and (5) it follows that

$$\mathbb{E}\big(\rho_S^{\mathrm{a}}(\mathbf{X}_i)\big) = \frac{m+1}{2}, \quad \mathbb{E}\big(\rho_S^{\mathrm{bd}}(\mathbf{X}_i)\big) = \frac{m^2+3m-4}{6}, \quad i = 1, \dots, m. \tag{6}$$

For simplicity, we assume that the number $m-1$ of forecast curves is high enough, so that we can neglect the different dependence structure of the observation curve when calculating the variance of the pre-rank function for the forecast curves. For the average ranking we obtain

$$\mathrm{Var}\big(\rho_S^{\mathrm{a}}(\mathbf{X}_i)\big) \approx \frac{m^2-1}{12d}, \qquad i = 1, \dots, m-1, \tag{7}$$

$$\mathrm{Var}\big(\rho_S^{\mathrm{a}}(\mathbf{X}_i)\big) = \frac{m^2-1}{12d} + \frac{(m-1)^2(d-1)}{12d}, \qquad i = m, \tag{8}$$

while the band depth ranking results in

$$\mathrm{Var}\big(\rho_S^{\mathrm{bd}}(\mathbf{X}_i)\big) \approx \frac{(m+1)(m-1)(7m^2+8m+12)}{60d}, \qquad i = 1, \dots, m-1, \tag{9}$$

$$\mathrm{Var}\big(\rho_S^{\mathrm{bd}}(\mathbf{X}_i)\big) = \frac{(m+1)(m-1)(7m^2+8m+12)}{60d} + \frac{(m^4-6m^3+13m^2-12m+4)(d-1)}{180d}, \qquad i = m. \tag{10}$$

Details of the derivations are given in the appendix.

That is, the variance of the pre-rank for the observation curve (which was assumed constant

over all components) is much larger than that of the forecasts curves (which were assumed independent across all components) for both pre-rank functions. It is thus more likely that we observe a very low or a very high pre-rank for the observation than for each ensemble member forecast which again leads to proportionally larger number of low and high ranks for the observation resulting in a $\cup$-shaped histogram.

4.1 Gaussian autoregressive processes

We now consider an example where $\mathbf{y} \in \mathbb{R}^d$ is a temporal trajectory of a real valued variable observed at d equidistant time points $t = 1, \ldots, d$. That is, the observation is a realization of a zero-mean Gaussian AR(1) (autoregressive) process $\mathbf{Y}$ with

$$\text{Cov}(Y_i, Y_j) = \exp(-|i - j|/\tau), \quad \tau > 0. \tag{11}$$

The process $\mathbf{Y}$ thus has standard Gaussian marginal distributions while the parameter τ controls how fast correlations decay with time lag. We set $\tau = 3$ for $\mathbf{Y}$ and consider ensemble forecasts of the same type but with a different parameter value τ. It follows from this construction that a univariate calibration test at a fixed time point would not detect any miscalibration in the forecasts.

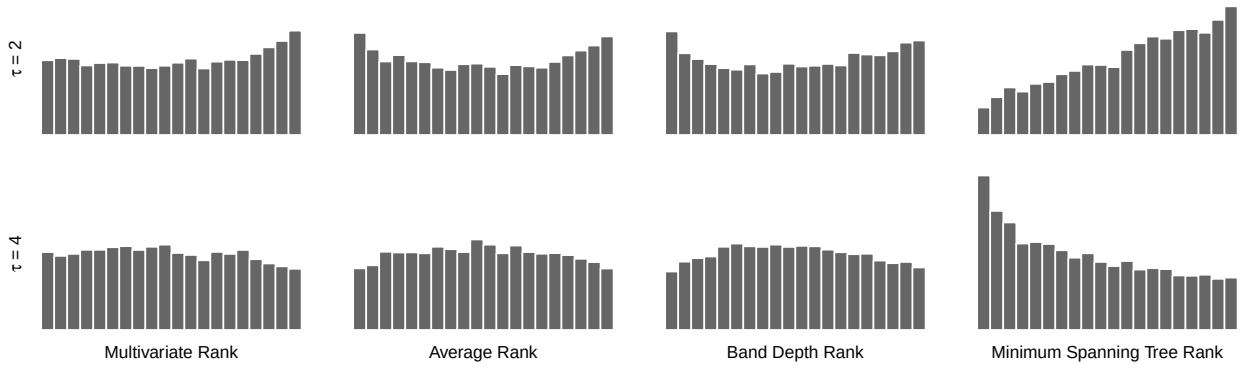

Figure 6: Simulation study to compare the sensitivity of the multivariate rank histogram, the band depth rank histogram and the average rank histogram to misspecification of the dependence structure. The observations follow an AR(1) process at time $t = 1, \ldots, 5$ with the dependence structure given in (11) for $\tau = 3$ while the ensemble forecasts follow the same model with $\tau = 2$ (top row) and $\tau = 4$ (bottom row). The results are based on 10000 repetitions with 19 ensemble members in each iteration.

Rank histograms for $d = 5$ and $m = 20$ where the forecast model has either $\tau = 2$ or $\tau = 4$ are shown in Figure 6. While all four calibration assessment methods are able to detect the miscalibration, the multivariate rank histogram suffers from identifiability issues with many low and identical pre-ranks resulting in a flattening out of the left side of the histograms. The band depth and the average rankings, on the other hand, seem quite sensitive to the model misspecification resulting in $\cup$-shape histograms when the correlations decay too fast in the forecasts and $\cap$-shaped histograms in the opposite situation. Here, the minimum spanning tree histogram gives the clearest indication of miscalibration.

Tables 1 and 2 demonstrate the effect of dimensionality and ensemble size on the average and band depth rank histograms in Figure 6. That is, we report the mean rank and the rank variance for both the observation and a randomly selected ensemble member under the two ranking methods when the observation follows the model in (11) with $\tau = 3$ while $\tau = 2$ for the forecasts. This example is similar to the example at the beginning of this section which can be considered the extreme case with $\tau = \infty$ for the observation and $\tau = 0$ for the forecast.

In the current example, dimensionality has only a minimal effect on the results while the size of the ensemble substantially affects the resulting values due to the varying number of possible ranks. As the serial dependence of the forecasts is too weak, the forecast ranks concentrate more strongly around the mean than the obseration ranks resulting in $\cup$-shaped histograms as those displayed in the top row of Figure 6. This difference in the rank variance appears to be somewhat stronger for the average ranking than for the band depth ranking. For the band depth ranking, we moreover observe a slight shift of the mean rank. This follows from the fact that the distribution of the band depth rank, a quadratic function of the univariate ranks, is slightly skewed such that difference in the variance of the pre-ranks may cause differences in the mean rank.

When the forecast model has the parameter value $\tau = 4$ as displayed in the bottom row of Figure 6, we observe similar effects of dimensionality and ensemble size as those reported in Tables 1 and 2. However, as this example has too strong serial dependence in the forecasts, the rank variance of the observations is here lower than that of the forecasts (results not shown).

Table 1: Mean ranks over 30000 repetitions for average ranking and band depth ranking under a zero-mean Gaussian AR(1) model with the exponential covariance function in (11) with $\tau = 3$ for the observation and $\tau = 2$ for the forecasts.

	Average				Band depth			
	$m = 20$	$m = 100$	$m = 200$	$m = 500$	$m = 20$	$m = 100$	$m = 200$	$m = 500$
Observation								
$d = 5$	10.5	50.4	100.0	251.5	10.7	51.7	102.2	256.8
$d = 100$	10.6	50.4	101.0	250.8	10.6	50.8	101.7	253.2
$d = 200$	10.5	50.4	100.2	251.2	10.5	50.9	101.8	251.5
$d = 500$	10.5	50.7	100.3	249.7	10.5	50.9	100.9	251.4
Randomly selected ensemble member								
$d = 5$	10.5	50.7	100.4	249.5	10.5	50.6	100.6	248.6
$d = 100$	10.5	50.7	101.3	250.7	10.5	50.2	100.5	251.1
$d = 200$	10.5	50.3	100.4	250.7	10.5	50.3	100.5	252.3
$d = 500$	10.5	50.3	100.4	250.6	10.5	50.5	100.4	251.2

Table 2: Rank variance over 30000 repetitions for average ranking and band depth ranking under a zero-mean Gaussian AR(1) model with the exponential covariance function in (11) with $\tau = 3$ for the observation and $\tau = 2$ for the forecasts.

	Average				Band depth			
	$m = 20$	$m = 100$	$m = 200$	$m = 500$	$m = 20$	$m = 100$	$m = 200$	$m = 500$
Observation								
$d = 5$	37	940	3773	23428	37	946	3749	23690
$d = 100$	40	1004	4042	25431	38	989	3982	24604
$d = 200$	39	1006	4002	25524	38	984	3949	24747
$d = 500$	39	1014	4052	25629	38	992	3965	24891
Randomly selected ensemble member								
$d = 5$	33	830	3319	20849	33	835	3341	20891
$d = 100$	33	837	3323	20663	33	825	3331	20715
$d = 200$	33	828	3316	21008	33	833	3315	20920
$d = 500$	33	833	3320	20763	33	835	3336	20825

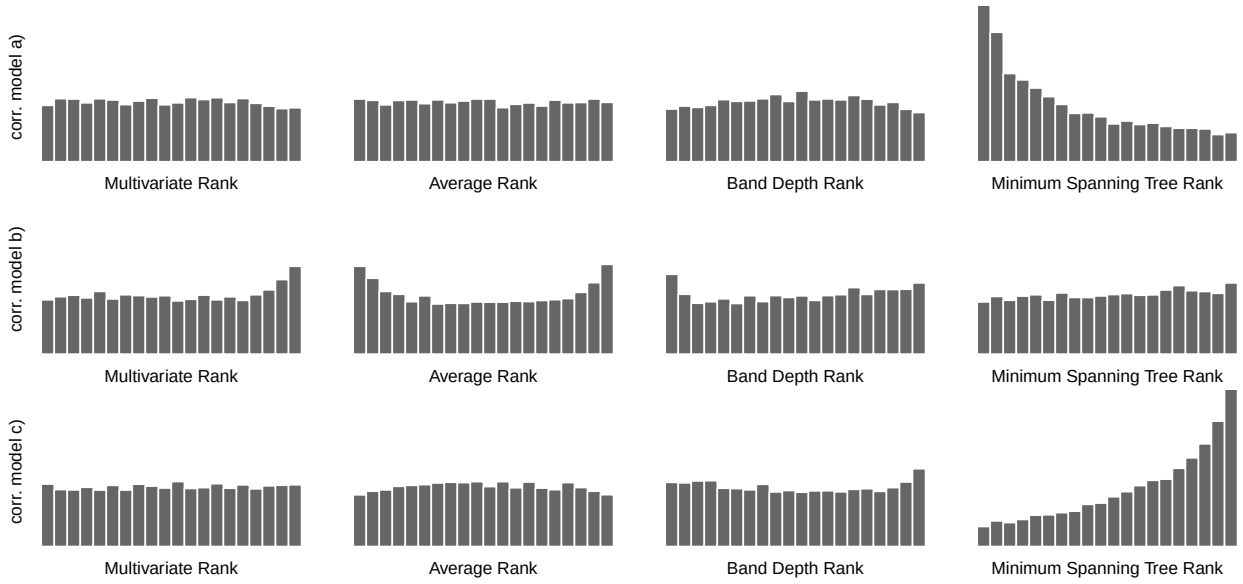

Figure 7: Simulation study to compare the sensitivity of the four multivariate ranking methods to miscalibration in the dependence structure. The observations follow the correlation models a), b), or c) (from top to bottom) at time $t = 1, \ldots, 15$ while the forecasts follow an AR(1) process with scale parameter $\tau = 3$. The results are based on 10000 repetitions with an ensemble of size 19.

4.2 Autoregressive vs. more complex correlation functions

Here, we consider Gaussian processes on $t = 1, \ldots, d$ where the observation follows the model in (11) with $\tau = 3$ while the components of the observation curve have a more complex correlation structure. That is, we consider the correlation models

a) $\text{Cov}(Y_i, Y_j) = \exp(-|i-j|/4.5)\big(0.75 + 0.25\cos(\pi|i-j|/2)\big)$

b) $\text{Cov}(Y_i, Y_j) = \big(1 + |i-j|/2.5\big)^{-1}$

c) $\text{Cov}(Y_i, Y_j) = \mathbb{1}\big\{|i-j| \leq 5\big\}\big(1 - |i-j|/5\big)$

Correlation function a) is a damped cosine that oscillates around the exponential model (11) with $\tau = 3$. The correlation functions b) and c) differ from this exponential model in that they have much stronger correlations at larger time lags, or zero correlations for larger time lags, respectively.

Figure 7 shows the resulting histograms for $d = 15$ and $m = 20$. When the observations follow correlation model a), the univariate ranks cancel out by averaging which results in a flat average rank histogram, while the minimum spanning tree histogram detects the false correlation

structure very well and the band depth rank histogram also indicates miscalibration. For the long range dependence model the opposite situation occurs in that the average rank histogram gives the clearest indication of miscalibration while the minimum spanning tree histogram is almost flat.

The last model c) with zero correlations beyond lag 5 finally presents a situation where the average rank and band depth rank histograms behave in the opposite way, the former being slightly $\cap$-shaped and the latter being slightly $\cup$-shaped. This suggests that the average rank histogram is more strongly affected by correlations at larger lags (which are overpredicted here) while the band depth rank histogram and the minimum spanning tree histogram are more sensitive to misspecifications of correlations at short lags (which are underpredicted here).

`R` code to recreate all the examples in this and the previous section is available in the online supplementary material.

5 Calibration of temperature forecast trajectories

We illustrate the use of the multivariate verification tools discussed above in the setting of probabilistic weather forecasting, where ensembles of weather predictions for the same location, time and weather variable are generated in order to represent forecast uncertainty (Palmer, 2002; Gneiting and Raftery, 2005; Schefzik et al., 2013). Specifically, we consider ensemble temperature forecasts at Berlin Tegel issued by the ensemble prediction system (EPS) of the European center for medium-range weather forecasts (ECMWF) with lead times of 6h, 12h, ..., 72h (Molteni et al., 1996; Leutbecher and Palmer, 2008). The EPS is initialized at 0000 UTC, consists of 50 ensemble members, and will be evaluated during the period from October 10, 2010 to December 31, 2012 using observational data from the local meteorological station as the truth.

The ECMWF forecasts used here are freely available from the TIGGE repository at `http://apps.ecmwf.int/datasets/data/tigge/`. The temperature observation data for Berlin Tegel and the `R` code needed to perform the analysis discussed below is provided in the online supplementary material.

The univariate rank histograms (not shown here) suggest that these raw ensemble forecasts have a systematic under forecasting bias at Berlin Tegel and are underdispersive at all considered lead times. We use a simple post-processing method to remove bias and adjust the ensemble spread for each lead time separately. Denoting by $\bar{\mathrm{x}}$ the mean of the 50 ensemble members (this is a vector with 12 components, one for each lead time) we obtain a bias-corrected mean μ by fitting a linear regression model $\mu_i = a_i + b_i \bar{x}_i$, separately for each component, to the corresponding observations y_i. For each forecast day the preceding 50 days are taken as training data so that we always have 50 forecast-observation pairs to fit the regression model. This is a compromise between flexible adaptation to seasonal changes on the one hand and gathering sufficient data to permit stable model fitting on the other hand, see e.g. Gneiting et al. (2005) and Raftery et al. (2005).

To adjust the ensemble spread, we use the "error dressing" approach of Roulston and Smith (2003), building a new ensemble by sampling from the errors $\varepsilon_{ij} = y_{ij} - \mu_{ij}$ of the bias-corrected forecasts on the respective training days $j = 1, \ldots, 50$ for lead time $i = 1, \ldots, 12$. To create an ensemble that appropriately represents the prediction uncertainty we additionally inflate ε_{ij} to adjust for the uncertainty in the bias correction (Faraway, 2004, Section 3.5). The ensemble obtained in this way is unbiased and nearly calibrated for individual lead times, see Figure 8.

We then consider three different strategies to model dependencies of forecast errors at different lead times,

(i) ignore multivariate dependencies and perform the error dressing separately for each lead time;

(ii) perform the error dressing separately for each lead time but use empirical copula coupling (ECC, Schefzik et al., 2013) in a second step to transfer the dependence structure from the raw ECMWF ensemble to the error dressing ensemble;

(iii) draw the errors from a zero-mean multivariate normal distribution with the empirical covariance matrix of the forecast errors over all lead times, where the variance is inflated as suggested above.

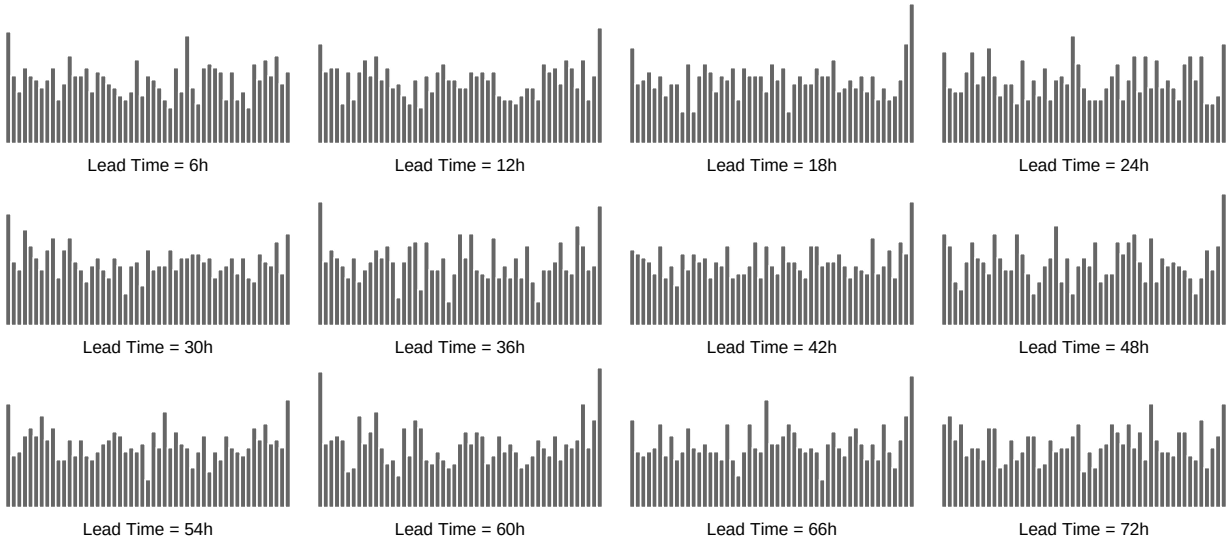

Figure 8: Univariate rank histogram of the bias-corrected error dressing forecasts for lead times 6h, 12h, ..., 72h at Berlin Tegel, each of them based on 823 verification days.

While all three strategies result in similar marginal distributions, the multivariate calibration assessment in Figure 9 reveals substantial differences. When the statistical postprocessing is performed independently for each lead time, the average rank histogram exhibit a $\cup$-shape indicating a lack of correlation between lead times in the forecasts. The band depth rank histogram is skew towards the lowest ranks indicating that the forecasts are too outlying on average and both the minimum spanning tree and the multivariate rank histograms are skewed towards the higher ranks. However, as the average rank histogram is symmetric, we would expect the outlying observation curves to have both too low ranks as well as too high ranks on average. We thus observe here a flattening out of the lower ranks in the multivariate rank histogram due to degeneracy in the pre-ranking; on any given day, at least half the curves are assigned a multivariate pre-rank of 1.

The ECC multivariate postprocessing of Schefzik et al. (2013) significantly improves the calibration of the independent postprocessing, though the observation curves are still somewhat too outlying. For the multivariate normal error sampling, the histograms appear quite close to uniform with a minor divergence towards a $\cup$-shape in both the minimum spanning tree rank histogram and the average rank histogram. An alternative forth multivariate postprocessing option is to apply univariate normal error models followed by ECC. This option leads to calibration results nearly

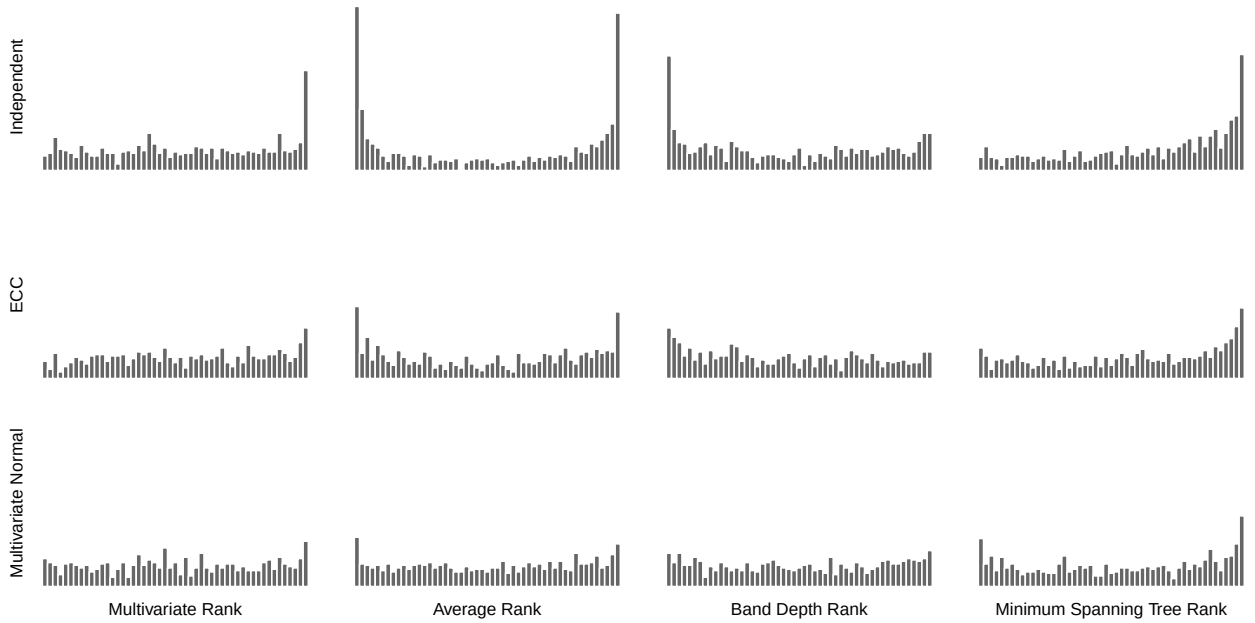

Figure 9: Multivariate rank histograms (left), band depth rank histograms (middle) and average rank histograms (right) of the bias-corrected error dressing forecasts with independent error sampling (top), under ECC (middle) and with multivariate normal error sampling (bottom). The results are based on forecasts for 12 lead times on 823 verification days at Berlin Tegel.

identical to the current results for ECC.

6 Discussion

In this paper, we propose two new methods for assessing the calibration of multivariate forecasts where the predictive distribution is represented by a forecast ensemble. Band depth ranking is based on the concept of band depth for functional data, originally proposed by López-Pintado and Romo (2009) and previously employed to create box plots for functional data (Sun and Genton, 2011, 2012; Sun et al., 2013). The somewhat simpler alternative, average ranking, employs the average over the univariate ranks. As demonstrated in several simulated and real data examples, both methods seem to correctly identify various sources of miscalibration in the forecast. Furthermore, they escape the curse of dimensionality affecting the multivariate ranking of Gneiting et al. (2008) as e.g. discussed by Pinson and Girard (2012). The minimum spanning tree ranking of Smith and Hansen (2004) and Wilks (2004) can be more sensitive to misspecifications than the new methods

proposed here. However, the resulting histograms seem to provide less information on the type of misspecification.

The band depth concept of López-Pintado and Romo (2009) is but one of a multitude of statistical depth functions for multivariate data that provide a center-outward ordering of the data (Zuo and Serfling, 2000). While we have here chosen the band depth due to its computational efficiency and interpretability of the resulting histograms, other depth functions might be equally appropriate for this purpose. As the band depth ranking assesses the centrality of the observation within the forecast ensemble, the sign of a potential bias cannot be learned from the shape of the histogram. Average ranking, on the other hand, distinguishes between positive and negative bias and effects where the forecasts exhibit a positive bias in a subset of the dimensions and a negative bias in a different subset might cancel out. Such effects can, however, easily be detected through univariate calibration assessment in each dimension.

Our examples, in particular the examples in Section 4.2, suggest that there is no single best pre-ranking method as all the methods may fail in detecting miscalibration. These methods project the multivariate quantity on a different univariate aspect and, in the process, lose information on other aspects. Our overall recommendation is thus to study histograms of different type before drawing conclusions. Furthermore, multivariate techniques should first and foremost complement univariate methods by effectively detecting features of miscalibration that cannot be found by studying the marginal distributions only. Conversely, ensuring marginal calibration in a first step can rule out the possibility of some compensating effects e.g. of marginal variances and correlations between different components.

Multivariate ranks relate to the multi-dimensional Smirnov two sample test proposed by Bickel (1969). Formal tests of uniformity can also be applied to the resulting ranks and this has been studied by several authors for univariate PIT or rank histograms, see e.g. Gneiting et al. (2007) and references therein. However, as dicussed by both Hamill (2001) and Gneiting et al. (2007), the use of formal tests is often complicated by the intricate dependence structures between the individual forecast cases. This holds, in particular, for partially overlapping forecast trajectories as discussed

in Section 5 or spatially aggregated forecasts.

Although calibration is an essential feature of a skillful forecast, a general forecast verification framework should consider a number of different aspects. Gneiting et al. (2007) state that the goal of probabilistic forecasting is to "maximize the sharpness with respect to calibration". That is, given a group of forecasts that all appear close to calibrated, we should choose the forecast with the highest information content. For predictive distributions or forecast ensembles, this can be attained by choosing the forecast with the smallest spread. More generally, proper scoring rules offer a verification framework under which various aspects of the forecast can be assessed, including calibration and sharpness. A comprehensive review of proper scoring rules is given in Gneiting and Raftery (2007).

Acknowledgments

We thank Marc Genton, Tilmann Gneiting, Alex Lenkoski, Roman Schefzik and Bert Van Schaeybroeck for sharing their thoughts and expertise. The temperature observation data for Berlin Tegel was kindly provided by the German Weather Service. The work of Thordis L. Thorarinsdottir was supported by Statistics for Innovation, *sfi*^{2}, in Oslo. The work of Michael Scheuerer was supported by the German Federal Ministry of Education and Research, in the framework of the extramural research program of the German Weather Service.

Supplementary materials

R code: `R` code to recreate all figures and tables in the paper along with general functions to calculate ranks under all four pre-ranking methods. (CreateFiguresAndTables.R)

Temperature observation data: Temperature observations for Berlin Tegel from August 1, 2010 to January 31, 2013 with a temporal resolution of 3 hours. (temp.obs.Rdata)

References

Anderson, J. L. (1996). A method for producing and evaluating probabilistic forecasts from ensemble model integrations. *Journal of Climate 9*, 1518–1530.

Bickel, P. J. (1969). A distribution free version of the smirnov two sample test in the p-variate case. *Annals of Mathematical Statistics 40*, 1–23.

Czado, C., T. Gneiting, and L. Held (2009). Predictive model assessement for count data. *Biometrics 65*, 1254–1261.

Dawid, A. P. (1984). Statistical theory: The prequential approach (with discussion and rejoinder). *Journal of the Royal Statistical Society Ser. A 147*, 278–292.

Faraway, J. J. (2004). *Linear Models with R*. Chapman & Hall/CRC.

Gneiting, T., F. Balabdaoui, and A. E. Raftery (2007). Probabilistic forecasts, calibration and sharpness. *Journal of the Royal Statistical Society Ser. B 69*, 243–268.

Gneiting, T. and A. E. Raftery (2005). Weather forecasting with ensemble methods. *Science 310*, 248–249.

Gneiting, T. and A. E. Raftery (2007). Strictly proper scoring rules, prediction, and estimation. *Journal of the American Statistical Association 102*, 359–378.

Gneiting, T., A. E. Raftery, A. H. Westveld, and T. Goldman (2005). Calibrated probabilistic forecasting using ensemble model output statistics and minimum CRPS estimation. *Monthly Weather Review 133*, 1098–1118.

Gneiting, T., L. I. Stanberry, E. P. Grimit, L. Held, and N. A. Johnson (2008). Assessing probabilistic forecasts of multivariate quantities, with applications to ensemble predictions of surface winds (with discussion and rejoinder). *Test 17*, 211–264.

Hamill, T. M. (2001). Interpretation of rank histograms for verifying ensemble forecasts. *Monthly Weather Review 129*, 550–560.

Hamill, T. M. and S. J. Colucci (1997). Verification of Eta-RSM short-range ensemble forecasts. *Monthly Weather Review 125*, 1312–1327.

Kruskal, J. B. (1956). On the shortest spanning subtree of a graph and the traveling salesman problem. *Proceedings of the American Mathematical Society 7*, 48–50.

Leutbecher, M. and T. N. Palmer (2008). Ensemble forecasting. *Journal of Computational Physics 227*, 3515–3539.

Lichtenstein, S., B. Fischhoff, and L. Phillips (1977). Calibration of probabilities: The state of the art. In H. Jungermann and G. Zeeuw (Eds.), *Decision Making and Change in Human Affairs*, Volume 16 of *Theory and Decision Library*, pp. 275–324. Springer Netherlands.

Liu, R. (1990). On a notion of data depth based on random simplices. *The Annals of Statistics 18*, 405–414.

López-Pintado, S. and J. Romo (2009). On the concept of depth for functional data. *Journal of the American Statistical Association 104*, 718–734.

Möller, A., A. Lenkoski, and T. L. Thorarinsdottir (2013). Multivariate probabilistic forecasting using ensemble Bayesian model averaging and copulas. *Quarterly Journal of the Royal Meteorological Society 139*, 982–991.

Molteni, R., R. Buizza, T. N. Palmer, and T. Petroliagis (1996). The new ECMWF ensemble prediction system: Methodology and validation. *Quarterly Journal of the Royal Meteorological Society 122*, 73–119.

Palmer, T. N. (2002). The economic value of ensemble forecasts as a tool for risk assessment: From days to decades. *Quarterly Journal of the Royal Meteorological Society 128*, 747–774.

401 Pinson, P. (2013). Wind energy: Forecasting challenges for its operational management. *Statistical*
402 *Science 28*(4), 564–585.

403 Pinson, P. and R. Girard (2012). Evaluating the quality of scenarios of short-term wind power
404 generation. *Applied Energy 96*, 12–20.

405 R Core Team (2013). *R: A Language and Environment for Statistical Computing*. Vienna, Austria:
406 R Foundation for Statistical Computing.

407 Raftery, A. E., T. Gneiting, F. Balabdaoui, and M. Polakowski (2005). Using Bayesian model
408 averaging to calibrate forecast ensembles. *Monthly Weather Review 133*, 1155–1174.

409 Roulston, M. S. and L. A. Smith (2003). Combining dynamical and statistical ensembles. *Tellus*
410 *A 55*, 16–30.

411 Schefzik, R., T. L. Thorarinsdottir, and T. Gneiting (2013). Uncertainty quantification in complex
412 simulation models using ensemble copula coupling. *Statistical Science 28*(4), 616–660.

413 Schuhen, N., T. L. Thorarinsdottir, and T. Gneiting (2012). Ensemble modlel output statistics for
414 wind vectors. *Monthly Weather Review 140*, 3204–3219.

415 Smith, L. A. and J. A. Hansen (2004). Extending the limits of ensemble forecast verification with
416 the minimum spanning tree. *Monthly Weather Review 132*, 1522–1528.

417 Sun, Y. and M. Genton (2012). Adjusted functional boxplots for spatio-temporal data visualization
418 and outlier detection. *Environmetrics 23*, 54–64.

419 Sun, Y. and M. G. Genton (2011). Functional boxplots. *Journal of Computational and Graphical*
420 *Statistics 20*, 313–334.

421 Sun, Y., M. G. Genton, and D. W. Nychka (2013). Exact fast computation of band depth for large
422 functional dataset: How quickly can one million curves be ranked? *Stat 1*, 68–74.

Wilks, D. S. (2004). The minimum spanning tree histogram as verification tool for multidimensional ensemble forecasts. *Montly Weather Review 132*, 1329–1340.

Ziegel, J. F. and T. Gneiting (2013). Copula calibration. arXiv:1307.7650.

Zuo, Y. and R. Serfling (2000). General notion of statistical depth function. *The Annals of Statistics 28*(2), 461–482.

Appendix

We consider here the special case where the components of the forecast curves are independent while the components of the observation curves are fully dependent (i.e. identical). As usual, we also assume that all curves are independent. Let X_{ik} be the random variable corresponding to the kth component of curve i, f its density and F its cumulative distribution function for $k = 1, \dots, d$ and $i = 1, \dots, m$.The ranks rank(X_{mk}) are then also random quantities and can be written as

$$\text{rank}(X_{mk}) = \sum_{i=1}^{m} \mathbb{1}\{X_{ik} \leq X_{mk}\}.$$

Under the above assumptions, these quantities are uniformly distributed on $\{1, \dots, m\}$, and hence have mean $\frac{m+1}{2}$ and variance $\frac{m^2-1}{12}$ for every $k \in \{1, \dots, d\}$. The relations in (6) then easily follow.

To establish the expressions for $\mathrm{Var}(\rho_S^{\text{bd}}(\mathbf{X}_i))$ and $\mathrm{Var}(\rho_S^{\text{a}}(\mathbf{X}_i))$ for the pre-rank functions in (4) and (5), respectively, we proceed as follows. For $i = 1, \dots, m-1$, we assume that

$$\mathrm{Var}\big(\rho_S^{\text{bd}}(\mathbf{X}_i)\big) \approx \frac{1}{d^2} \sum_{k=1}^{d} \mathrm{Var}\big((m+1)\text{rank}(X_{ik}) - \text{rank}(X_{ik})^2\big),$$

and similar for $\mathrm{Var}(\rho_S^{\text{a}}(\mathbf{X}_i))$. An application of Faulhaber's formula,

$$\sum_{i=1}^{m} i^3 = \frac{m^2(m+1)^2}{4}, \quad \sum_{i=1}^{m} i^4 = \frac{m(m+1)(2m+1)(3m^2+3m-1)}{30},$$

then leads to the results in (7) and (9).

Since X_{mk} takes the same value (almost surely) for all k, we can write $X_{mk} = X_{m*}$. By using the independence assumptions (between curves on the one hand and components of the forecast vectors on the other hand) we obtain for $k \neq k'$

$$\begin{aligned}
\mathbb{E}\big(\text{rank}(X_{mk})\text{rank}(X_{mk'})\big) &= \sum_{i=1}^{m}\sum_{i'=1}^{m} P\big(X_{ik} \leq X_{mk}, X_{i'k'} \leq X_{mk'}\big) \\
&= 1 + \frac{2(m-1)}{2} + \sum_{i=1}^{m-1}\sum_{i'=2}^{m-1} P\big(X_{ik} \leq X_{m*}, X_{i'k'} \leq X_{m*}\big) \\
&= m + \frac{(m-1)^2}{3}.
\end{aligned}$$

The last equality uses the independence of $X_{ik}, X_{i'k'}$, and X_{m*} which permits the calculation of the joint probability via Fubini,

$$P\big(X_{ik} \leq X_{m*}, X_{i'k'} \leq X_{m*}\big) = \int_{-\infty}^{\infty} \big(F(y)\big)^2 f(y)dy = \int_0^1 y^2 dy = \frac{1}{3}.$$

This finally yields

$$\text{Cov}\big(\text{rank}(X_{mk}), \text{rank}(X_{mk'})\big) = m + \frac{(m-1)^2}{3} - \frac{(m+1)^2}{4} = \frac{(m-1)^2}{12}, \qquad k \neq k',$$

from which we obtain equation (8).

The results for the band depth ranking in (10) addtionally require the calculation of

$$\begin{aligned}
\mathbb{E}\big(\text{rank}(X_{mk})\text{rank}(X_{mk'})^2\big) &= \frac{3m^3 + 4m^2 + 3m + 2}{12}, \\
\mathbb{E}\big(\text{rank}(X_{mk})^2\text{rank}(X_{mk'})^2\big) &= \frac{6m^4 + 9m^3 + 8m^2 + 3m + 4}{30}
\end{aligned}$$

which are obtained in a similar manner (but with many more cases).